SLAC PUB 8405

March 2000

A Small Particle Model as a Possible Explanation of Recently Reported Cavity Lights*

David Fryberger†

Stanford Linear Accelerator Center, MS 20
P.O. Box 4349
Stanford University
Stanford, California 94309

Abstract

Very unusual light phenomena have been observed inside superconducting niobium cavities under an electrical excitation equivalent to an average acceleration of ∼4 MV/m. Of particular interest is the observation of what appear to be objects executing elliptical orbits. A small particle model that yields a cylindrical harmonic oscillator potential well inside such a cavity is developed and appears to offer considerable promise as an analytical framework in which to understand these observations; the harmonic oscillator potential well has elliptical orbits as general solutions. However, explicit calculations indicate that with the cavity excitation parameters associated with this data, it is highly unlikely that a small object orbiting in such a potential well can be made of any known material. Deficiencies of the model are discussed, and avenues for further study, both theoretical and experimental, are indicated.

PACS: 46.90 +s; 52.80 Mg

Keywords: Field emission; Cavity lights

I. INTRODUCTION

Very unusual light emission phenomena in the interior of radio frequency (1.5 GHz) superconducting electron accelerator cavities have recently been reported [1]. These phenomena were observed with a CCD camera[1] viewing the interior of the cavities during the course

*Work Supported by Department of Energy Contract DE-AC03-76SF-00515.

†Tel. +1-650-926-2768, FAX: +1-650-926-2521, e-mail: fryberger@slac.stanford.edu

[1]Monochrome Micro Camera, Model H53004, Edmund Scientific Optics and Optical Instrument Catalogue N991A, 1999, p. 177.

of an investigation of the field emission limitation of superconducting niobium cavities. In these tests, the CCD camera was mounted in a vertical cryogenic test dewar looking up into the cavities along the cavity axis. (There were no electron beams involved in these tests.) Two such tests were made. The first was viewing the interior of a single cell cavity, and the second was viewing the interior of a production CEBAF five-cell cavity. Similar results were obtained in both tests. It was reported that: "Three general classes of glowing filaments were observed: 1) regular-shaped closed, 2) irregular-shaped closed, and 3) open."

Since the pressure in these cavities is so low (10^{-9} torr or less), any conventional plasma discharge would be very diffuse; as such it would be unable to give light from a small, well-defined volume. In many frames, reflections of the region of luminosity can clearly be seen in the cavity walls. These afford a quasi-stereo view and indicate that (in these instances) there is no wall contact by the source of the luminosity. Consequently, a plasma discharge appears to be ruled out.

Another possible explanation is that the observed luminosity emanates from a small particle. These small particles would be moving about inside the cavity, and occasionally getting trapped into closed orbits. Based upon the assumption that one is indeed observing small objects orbiting inside the cavity, the purpose of this paper is to develop an analytical model for such orbiting objects that can be used as a framework to try to understand the observations and also serve as a basis for future work, both experimental and theoretical.

II. HARMONIC OSCILLATOR POTENTIAL

A. Sphere Model

It is appropriate to begin the modeling effort with the simplest possible shape, a small sphere. For the sake of analysis, we shall assume that the the sphere is made of niobium, although other materials are possible. One can suppose that this niobium would be pulled off of the interior wall by electromagnetic forces, and that its spherical shape could be a result of melting by electrical currents at the time of formation.

Radial Force

We now show that a (Lorentz) restoring force leading to stable particle orbits will derive from the electromagnetic fields in the cavity acting upon a small conducting sphere. To do this, we first write the axial accelerating field vector as

$$\mathbf{E} = E_0 \mathbf{1_z} \cos\, \omega_a t, \tag{1}$$

where E_0 is the maximum magnitude of the rf accelerating field (in the center of the cavity along the cavity or beam axis)[2] at frequency $f_a = \omega_a/2\pi$ and $\mathbf{1_z}$ is the unit vector in the

[2]To the extent that the particle orbits are away from the center of the cavity, the $\mathbf{E}$ field will be reduced, but this reduction is minor–on the order of 5%, or less–for the observed orbits.

z-direction. (Gaussian units [2] are used here, and boldface type denotes three-vectors.) Using the cylindrical symmetry of the cavity and Maxwell's equations yields

$$\mathbf{B} = -\frac{\rho\ \omega_a\ E_0}{2c}\mathbf{1}_{\boldsymbol{\phi}}\ \sin\ \omega_a t, \tag{2}$$

where ρ is the usual (right handed) cylindrical coordinate, $\mathbf{1}_\phi$ is the unit vector in the ϕ direction, and c is the speed of light.

It is well known that an $\mathbf{E}$ field will induce an electric moment [3]

$$\boldsymbol{\mu} = \mathbf{E}\ a^3 \tag{3}$$

in a sphere of radius a, as depicted in Fig. 1. It is easy to show that this formula for $\boldsymbol{\mu}$ derives from a charge density of

$$\sigma = \frac{3E_0}{4\pi}\ \cos\theta \tag{4}$$

on the surface of the sphere [3]. Note that σ is independent of a. Eq. (4) leads to the charge on the positive hemisphere,

$$Q = \frac{3E_0 a^2}{4}, \tag{5}$$

which equation is included here for later reference.

Now $\boldsymbol{\mu}$ oscillates in phase with $\mathbf{E}$ for $a \ll \lambda_a$, the free-space wavelength of the accelerating power. One can see that in the presence of the magnetic field $\mathbf{B}$, which also oscillates coherently with $\mathbf{E}$ (but 90° out of phase), there will be a Lorentz force on this oscillating dipole:

$$\mathbf{F} = \frac{\dot{\boldsymbol{\mu}}}{c} \times \mathbf{B}. \tag{6}$$

Using Eqs. (1-3) in Eq. (6) yields

$$\mathbf{F} = -\frac{E_0^2\ \omega_a^2\ \rho\ a^3\ \mathbf{1}_{\boldsymbol{\rho}}}{2\ c^2}\ \sin^2\omega_a t. \tag{7}$$

Noting that $< \sin^2\omega_a t >= \frac{1}{2}$, Eq. (7) defines a (low frequency) restoring force constant (along the ρ direction),

$$k = \frac{E_0^2\ \omega_a^2\ a^3}{4c^2}, \tag{8}$$

for a two-dimensional cylindrical harmonic potential well centered on the z-axis.

Orbital Frequency

The (angular) frequency for a sphere oscillating (or orbiting) in this potential well is given by

$$\omega_o = \sqrt{\frac{k}{M}} = \frac{E_0}{2\lambda_a}\sqrt{\frac{3\pi}{\rho_M}}, \tag{9}$$

where M is the mass of the sphere and ρ_M is the mass density of the sphere. It is interesting to note that ρ_M is the only parameter of the sphere that enters into the determination of ω_o.

Solving Eq. (9) for ρ_M, and noting that $\omega_o = 2\pi f_o$, yields

$$\rho_M = \frac{3\pi\ E_0^2}{4\lambda_a^2\ \omega_o^2} = \frac{3E_0^2}{16\pi\lambda_a^2\ f_o^2}. \tag{10}$$

Using observed orbital frequencies, Eq. (10) will enable one to determine the sphere densities implied by this model.

Dielectric Sphere

In the interest of completeness, we consider a sphere made of a dielectric material characterized by a dielectric constant ϵ. In this case, Eq. (4) becomes [4]

$$\sigma = \frac{3}{4\pi}\left(\frac{\epsilon - 1}{\epsilon + 2}\right) \mathrm{E}_0\ \cos\theta, \tag{11}$$

and Eq. (5) becomes

$$Q = \frac{3}{4}\left(\frac{\epsilon - 1}{\epsilon + 2}\right)\ \mathrm{E}_0\ a^2. \tag{12}$$

Comparing Eqs. (11 and 12) to Eqs. (4 and 5) one can see that for the moment and charge calculations a conductor behaves like a dielectric material with an infinite dielectric constant, and that the force constant k of a dielectric sphere will always be less than that for a conducting sphere; for typical dielectrics of low ϵ, it will be considerably less.

Spherical Shell

As a sample calculation below will show, a solid sphere is too heavy to satisfy Eq. (10) using the f_o implied by Fig. 2a of Ref. [1], reproduced below as Fig. 7. As a solution to this difficulty, one can contemplate a spherical shell or bubble as the orbiting object. In this configuration the mass can be reduced while maintaining the same μ; the volume of the material in a thin spherical shell is $4\pi a^2 \Delta a$. However, another sample calculation, below, indicates that a spherical shell yielding the observed f_o would have an unrealistically thin shell thickness Δa.

Power Absorption

Since the orbiting objects do not appear to be in contact with the walls of the cavity and ionic currents are diffuse, incandescent spots can be ruled out as the source of luminosity. Hence, it is a reasonable deduction that the luminosity associated with the orbiting object is due to thermal heating and concomitant black (or gray) body radiation. Consequently, the question of power absorption by the orbiting sphere is relevant.

As an initial model to approach this question, imagine that the sphere is divided along the neutral plane and that an equivalent resistor is inserted to furnish a conducting path between the two hemispheres, as depicted in Fig. 2. An equivalent electrical circuit for this concept is shown in Fig. 3. The voltage of the power source derives from the accelerating gradient in the cavity, which is coupled into the surface of the sphere viewed as the capacitor C. To continue along this line, we use Eqs. (3 and 5) for the charge moment and the total induced charge on a hemisphere, respectively, and estimate the peak driving voltage in the equivalent circuit to be

$$V_0 = E_0 \frac{\mu}{Q} = \frac{4aE_0}{3}. \tag{13}$$

The capacitance is given by

$$C = \frac{Q}{V_0} = \frac{3E_0\ a^2/4}{4E_0\ a/3} = \frac{9a}{16}. \tag{14}$$

Looking at the equivalent circuit, one can see that the heating power in the sphere will be

$$P = I_0^2 R/2, \tag{15}$$

where

$$I_0 = \frac{V_0}{(R^2 + \frac{1}{\omega_a^2 C^2})^{1/2}}, \tag{16}$$

and the factor two in Eq. (15) converts the peak current I_0 into rms for the power calculation.

As one would expect, the power is null when $R = 0$ and when $R = \infty$. (Note intermediate values of R will cause some variation in the appropriate formula for V_0, but not enough to impair the conclusions of this analysis.) It is easy to show that the maximum power dissipation occurs when

$$R = \frac{1}{\omega_a C}. \tag{17}$$

Using Eqs. (16 and 17) in Eq. (15) yields

$$P_{max} = \frac{V_0^2 \omega_a C}{4} = \frac{a^3 \omega_a E_0^2}{4}. \tag{18}$$

If

$$R \ll \frac{1}{\omega_a \ C} \tag{19}$$

Then Eq. (16) becomes

$$I_0 = \omega_a \ C V_0. \tag{20}$$

That is, the current in the sphere is determined entirely by the capacitative coupling, independent of the intrinsic resistivity of the material in the sphere. That Eq. (19) is valid in the case of typical conductors will be justified below.

Assuming the validity of Eq. (19), the calculation of the power absorbed by a sphere is straightforward. Consider a Δz slice of a sphere as depicted in Fig. 4. The resistance in this slice

$$\Delta R = \frac{\rho_G \Delta z}{\pi \ a^2 \sin^2\theta}, \tag{21}$$

where ρ_G is the resistivity of the material (in Gaussian units). The current flowing through this slice

$$i(\theta, t) = q_0(\theta)\omega_a \ \sin(\omega_a t), \tag{22}$$

where

$$q_0(\theta) = \int_0^\theta \ 2\pi\sigma \ a^2 \sin\theta d\theta = \frac{3\mathrm{E}_0 \ a^2}{4}(1 - \cos^2\theta), \tag{23}$$

and Eq. (4) was used for σ. The power absorption

$$P = \int_0^a \left(\frac{3E_0\ a^2}{4}\right)^2\ \frac{\rho_G\ \sin^2\theta\ dz}{\pi a^2} = \frac{3E_0^2\ \omega_a^2\ a^3\ \rho_G}{8\pi}. \tag{24}$$

Using Eqs. (13, 14 and 20) to determine I_0 in Eq. (15) to calculate the absorbed power in terms of the equivalent lump sum resistance R, and comparing to Eq. (24), one finds

$$R = \frac{4\rho_G}{3\pi a}. \tag{25}$$

With this result, and using Eq. (14), Eq. (19) becomes

$$\rho_G \ll \frac{4\pi}{3\omega_a}, \tag{26}$$

independent of the radius of the sphere. Even graphite, which has a relatively large resistivity, easily satisfies Eq. (26). To verify this assertion, one can use Jackson [5] to convert the resistivity of graphite in mks units [6], $\rho_{mks} = 1.38 \times 10^{-5}\ \Omega$m, to Gaussian units. Taking this step one finds that $\rho_G = 1.53 \times 10^{-15}$ s for graphite, and Eq. (26) becomes

$$1.53 \times 10^{-15}\ \text{s} \ll 4.44 \times 10^{-10}\ \text{s}, \tag{26$'$}$$

justifying the use of Eq. (19) in the calculation of the power absorbed by a sphere of conducting material. Since the sample calculations given below indicate that neither the sphere nor the thin spherical shell appear to be viable candidates in this model, we omit explicit estimates of power absorption and temperature rise for these cases.

B. Needle Model

Electric Dipole Moment

A slender needle as the orbiting object would enable a given induced moment with a mass much less than that of a solid sphere. That is, mass reduction for the purpose of achieving satisfactory orbital parameters in this model can be accomplished by slendering as well as by hollowing. Exact analytical calculations for such a needle can be made using a prolate spheroid as a model for the needle. The prolate spheroidal coordinate system is $(\xi,\ \eta,\ \phi)$ [7]. As a practical matter, the fact that an orbiting object might more resemble a whisker than a prolate spheroid would imply a modest correction to the estimated aspect ratio to yield a given orbital frequency. But for the purposes of this paper, the prolate spheroid calculation will give results that adequately represent what can be expected in the case of a slender (linear) geometry.

In order to determine the induced μ in a prolate spheroid, we start with the voltage distribution in the region above a ground plane with an embedded (semi) prolate spheroidal boss [8], as shown in Fig. 5:

$$V = -E_z(a^2 - b^2)^{1/2}\xi\eta \left(1 - \frac{\coth^{-1}\eta - \frac{1}{\eta}}{\coth^{-1}\ \eta_0 - \frac{1}{\eta_0}}\right), \tag{27}$$

where

$$\eta_0 \equiv \frac{a}{(a^2 - b^2)^{1/2}} = \frac{1}{(1 - A_R^{-2})^{1/2}} \tag{28}$$

defines the spheroidal surface of the boss; a is the height of the boss and b is its radius at the ground plane, and $A_R \equiv a/b$ is the aspect ratio. The negative sign is inserted into Eq. (27) to accommodate the proper sign relationship between E_z and V. The next step is to find the gradient of V:

$$\mathbf{E} = -\boldsymbol{\nabla} V = -\frac{1}{h_\xi}\frac{\partial V}{\partial \xi}\ \mathbf{1}_\xi - \frac{1}{h_\eta}\ \frac{\partial V}{\partial \eta}\ \mathbf{1}_\eta - \frac{1}{h_\phi}\frac{\partial V}{\partial \phi}\ \mathbf{1}_\phi, \tag{29}$$

where h_ξ, h_η, and h_ϕ are the scale factors for the coordinates (ξ, η, ϕ), respectively. These scale factors [7],

$$h_\xi = (a^2 - b^2)^{1/2}\left(\frac{\eta^2 - \xi^2}{1 - \xi^2}\right)^{1/2}, \tag{30}$$

$$h_\eta = (a^2 - b^2)^{1/2}\left(\frac{\eta^2 - \xi^2}{\eta^2 - 1}\right)^{1/2}, \text{ and} \tag{31}$$

$$h_\phi = (a^2 - b^2)^{1/2}[(1 - \xi^2)(\eta^2 - 1)]^{1/2}, \tag{32}$$

are recorded for use below.

The $\mathbf{E}$ of interest is at the surface of the boss ($\eta = \eta_0$), and in this location the only nonzero component of $\boldsymbol{\nabla} V$ is E_η. Using Eqs. (27 and 31) in Eq. (29), one obtains

$$E_\eta = \frac{E_z(\eta^2 - 1)^{1/2}\xi}{(\eta^2 - \xi^2)^{1/2}}\left[1 - \frac{\coth^{-1}\eta - 1/\eta}{\coth^{-1}\eta_0 - 1/\eta_0} + \frac{1}{(\coth^{-1}\eta_0 - 1/\eta_0)\eta(\eta^2 - 1)}\right], \tag{33}$$

which on the surface of the spheroid ($\eta = \eta_0$) becomes

$$E_{\eta_0} = \frac{E_z\xi}{\eta_0(\eta_0^2 - \xi^2)^{1/2}(\eta_0^2 - 1)^{1/2}(\coth^{-1}\eta_0 - \frac{1}{\eta_0})}. \tag{34}$$

One can now find the surface charge σ through the relationship [9],

$$\mathbf{E} \cdot \mathbf{n} = 4\pi\sigma, \tag{35}$$

where $\mathbf{n}$ is the outward unit vector normal to the surface. That is,

$$\sigma = \frac{E_{\eta_0}}{4\pi} = \frac{E_z \xi}{4\pi\eta_0(\eta_0^2 - \xi^2)^{1/2}(\eta_0^2 - 1)^{1/2}(\coth^{-1}\eta_0 - 1/\eta_0)}. \tag{36}$$

The total charge on the surface of the boss, then, is

$$Q_b = \int_0^{2\pi} \int_0^1 \sigma h_\xi \; h_\phi \; d\xi \; d\phi, \tag{37}$$

and the induced electric moment in the boss is

$$\mu_b = \int_0^{2\pi} \int_0^1 z\sigma h_\xi \; h_\phi \; d\xi \; d\phi, \tag{38}$$

where

$$z = (a^2 - b^2)^{1/2} \; \eta \; \xi. \tag{39}$$

The total moment for an orbiting spheroid, μ, is twice that of the boss, and one derives

$$\mu = 2\mu_b = \frac{E_z \; a^3}{3\eta_0^3(\coth^{-1} \; \eta_0 - 1/\eta_0)}, \tag{40}$$

and

$$Q_b = \frac{E_z a^2}{4\eta_0^3(\coth^{-1}\eta_0 - 1/\eta_0)}. \tag{41}$$

One can see from Eqs. (28) and (40) that varying A_R will (though η_0) affect the induced moment as well as the total mass. It is easy to verify that as the prolate spheroid becomes a sphere ($b \to a$), Eqs. (40) and (41) become Eqs. (3) and (5), respectively.

Power Absorption and Luminosity

It is now possible to estimate the power absorption by the needle and the resulting equilibrium temperature. Proceeding as with the sphere, we see that V_0 is the same as for the sphere while

$$C = \frac{3a}{16\eta_0^3(\coth^{-1}\eta_0 - 1/\eta_0)}. \tag{42}$$

As one expects for $b \to a$, Eq. (42) $\to$ Eq. (14), the analogous equation for the sphere. Now consider a Δz slice of the prolate spheroid as indicated in Fig. 6. The resistance of this slice is

$$\Delta R = \frac{\rho_G \Delta z}{\pi \rho^2} = \frac{\rho_G \eta_0^2 \Delta \xi}{\pi a (1-\xi^2)\ (\eta_0^2 - 1)}, \tag{43}$$

where the right hand side has been converted to prolate spheroidal coordinates for the purposes of a subsequent integration. Assuming that Eq. (19) is satisfied, the charge on the cap of this spheroid, which each cycle will flow back and forth through this slice, is

$$q_0(\xi) = \frac{E_z a^2 (1-\xi^2)}{4\eta_0^3 (\coth^{-1}\eta_0 - 1/\eta_0)}, \tag{44}$$

which for $\xi \to 0$ yields Eq. (41), as expected.

The power absorbed by the prolate spheroid, then, is

$$P = \int (\omega_a q_0)^2\ dR = \frac{A_R^2\ \omega_a^2\ E_z^2 a^3 \rho_G}{24\pi\ \eta_0^6 (\coth^{-1}\eta_0 - 1/\eta_0)^2}, \tag{45}$$

where the range of integration is over the upper half of the prolate spheroid. [There are cancelling factors of two in Eq. (45).] Equating this result to the power in the equivalent circuit, Eq. (15), leads to the equivalent resistance

$$R = \frac{4 A_R^2\ \rho_G}{3\pi a}, \tag{46}$$

which for the sphere ($A_R = 1$) yields Eq. (25). Similarly, Eq. (26) becomes

$$\rho_G \ll \frac{4\pi\ \eta_0^3 (\coth^{-1}\eta_0 - 1/\eta_0)}{A_R^2 \omega_a} \tag{47}$$

for the prolate spheroid. That Eq. (47) is satisfied will be shown below.

It is now straightforward to derive the equation for the equilibrium temperature assuming that power absorption from the cavity field is in equilibrium with radiated gray body radiation. Gray body radiation power is given by [10]

$$P_{rad} = A \epsilon_r \sigma_s T^4, \tag{48}$$

where A is the surface area, ϵ_r is the emissivity relative to a black body ($\epsilon_r = 1$ denotes a black body.), and

$$\sigma_s = 5.67 \times 10^{-5} \frac{\text{ergs}}{\text{s cm}^2\text{K}^4} \tag{49}$$

is the Stefan-Boltzmann constant. For slender prolate spheroids, it is easy to show that

$$A \cong \frac{\pi^2 ab}{2}. \tag{50}$$

Assuming a uniform surface temperature, and equating Eqs. (45) and (48), the condition for equilibrium becomes

$$\frac{A_R^2 \; a^3 \; \omega_a^2 \; E_z^2 \; \rho_G}{24\pi \; \eta_0^6 (\coth^{-1}\eta_0 - 1/\eta_0)^2} = \frac{\pi^2 ab}{2} \epsilon_r \sigma_s T^4. \tag{51}$$

Solving Eq. (51) for T yields

$$T = \left[\frac{A_R^3 \; a \; \omega_a^2 \; E_z^2 \; \rho_G}{12\pi^3 \; \epsilon_r \; \sigma_s \; \eta_0^6 (\coth^{-1}\eta_0 - 1/\eta_0)^2} \right]^{1/4}. \tag{52}$$

It is evident from Eq. (52) that larger objects, and more slender objects, will attain higher equilibrium temperatures, and that the functional dependence upon aspect ratio is much stronger than the dependence on size.

A Dielectric Needle

One more possibility for the needle model deserves consideration: a dielectric needle. The interior electric field in a prolate spheroid, of dielectric constant ϵ, is given by [11]

$$E_{int} \;=\; \frac{E_0}{\epsilon - (\epsilon - 1)\eta_0 \left[(1 - \eta_0^2)\coth^{-1}\eta_0 + \eta_0 \right]}. \tag{53}$$

Using the boundary conditions at the surface of a dielectric prolate spheroid, one obtains an equivalent surface polarization charge

$$\sigma = (\epsilon - 1) \frac{E_{int} \xi (\eta_0^2 - 1)^{1/2}}{4\pi (\eta_0^2 - \xi^2)^{1/2}}, \tag{54}$$

which, using Eq. (53), enables a calculation of the (equivalent polarization) charge on the hemispheroid:

$$Q_b = \int_0^{2\pi} \int_0^1 \sigma h_\xi \; h_\phi \; d\xi \; d\phi = \frac{(\epsilon - 1) a^2 (\eta_0^2 - 1) E_0}{4\eta_0^2 \left\{ \epsilon + (\epsilon - 1)\eta_0 \left[(\eta_0^2 - 1)\coth^{-1}\eta_0 - \eta_0 \right] \right\}}. \tag{55}$$

One can demonstrate that Eq. (55) satisfies two limits of interest: 1) $\epsilon \to \infty$, which recovers the charge on a conducting prolate spheroid, Eq. (41), and $\eta_0 \to \infty$, which recovers the charge on a dielectric hemisphere, Eq. (12).

III. SAMPLE CALCULATIONS

A. Orbital Frequency

Fig. 2a of Ref. (1) is reproduced here as Fig. 7, where the major axis of the orbit ellipse is indicated. Since a full ellipse is seen, one can immediately deduce that $f_o \geq 60$ Hz. (The light level in the cavity is low, which will result in the shutter open time to be at its nominal maximum of $1/60^{\text{th}}$ s.)[1] The higher luminosity abutting points A and B in Fig. 7 is due to overlapping orbital paths and indicates that these points are the termini of the orbit segment as viewed by the camera in $1/60^{\text{th}}$ s. The location of points A and B enables an improved estimate for f_o. First note that the orbital motion is sinusoidal along both the major and minor axes. This sinusoid (for the major axis) is plotted in Fig. 8, where points A and B have been determined by the orbital sine function derived from the displacements from the minor axis of points A and B in Fig. 7. ($\sin\theta_A = 0.887$ and $\sin\theta_B = 0.873$.) Thus, $\theta_A = 62°$ and $\theta_B = 61°$, and

$$f_o = \frac{62 + 360 + 61}{360} \times 60 \cong 80 \text{ Hz}. \tag{56}$$

B. Sphere

This result for f_o can be used in Eq. (10) to determine the ρ_M that this model will require of the object (if it is a sphere) orbiting in Fig. 7. To make a calulation, we can estimate E_0 from the average accelerating gradient (of 4 MV/m) by assuming that a beam electron experiences two sine factors as it traverses the cavity, one for space variation and one for time-variation. This assumption (numerically verified by an explicit SUPERFISH calculation) leads to

$$E_0 = 2\bar{E}_a = 8 \times 10^6 \text{ V/m} = 267 \frac{\text{statV}}{\text{cm}}. \tag{57}$$

Using Eqs. (56) and (57) in Eq. (10) yields

$$\rho_M \simeq 0.00166 \text{ g/cm}^3. \tag{58}$$

The low sphere density indicated by Eq. (58) signals a significant difficulty; it is not evident what (solid) material would be available to satisfy this density requirement. This estimated ρ_M is considerably less than that of styrofoam or the very light silica aerogels that are used in Čerenkov particle detectors [12]; in fact, it is not much more dense than air (which at STP has a density of ~ 0.0012 g/cm^3) [13]. And the correction to this result associated with the off-axis reduction of the **E** field[2] will not make a qualitative change in the above conclusion.

C. Spherical Shell

To construct a spherical shell out of niobium ($\rho_M = 8.55$ g/cm^3) to give the requisite effective density for $f_o = 80$ Hz would call for a density reduction by a factor $8.55/0.00166 \sim 5200$. This means that the shell thickness would have to be $\sim 6 \times 10^{-5}$ of the shell radius. For example, a spherical shell of 1 mm in diameter would have a shell thickness of ~ 0.03 μm. While such an object is conceivable, it is difficult to imagine how it could be created by an uncontrolled process inside a beam cavity, or be some kind of debris associated with the history of the cavity. And postulating a material of lower ρ_M than niobium would not qualitatively change this conclusion. A spherical shell of a dielectric material is also ruled out; it will have a much reduced induced electric moment because in a dielectric the induced moment is a volume effect. Thus, we see that the density requirement of Eq. (10) is so stringent that a sphere or spherical shell of any known material appears to be precluded as a candidate (in this model) for the orbiting object. Even a sizable underestimate of E_0 (by a factor of two or three, say) does not enable any known candidate materials to satisfy the (higher) density estimate.

D. Needle

To determine a suitable A_R for an orbiting needle, one first needs to determine how (the formula for) ω_o varies as a function of A_R. First, we use Eqs. (3, 28 and 40) to plot the ratio μ_{ps}/μ_s as a function of A_R (and fixed a) in Fig. 9, which indicates that with increasing A_R, μ_{ps} drops with respect to μ_s but not very fast. Then, using the volume of the prolate spheroid,

$$V_{ps} = \frac{4\pi}{3}\, ab^2 = \frac{4\pi\, a^3}{3A_R^2}, \tag{59}$$

we plot as function of A_R (and fixed a) the enhancement ratio $R_E \equiv \dfrac{\mu_{ps}/\mu_s}{V_{ps}/V_s}$ in Fig. 10. R_E takes into account the variation of both the moment and the volume as a function of A_R.

To establish the requisite A_R, recall from the above sphere analysis that $R_E \sim 5200$ was required to make a sperical shell light enough to orbit at 80 Hz. This same enhancement factor is required for a prolate spheroid (of niobium) to satisfy the orbit frequency criterion. The curve plotted in Fig. 10 indicates that a prolate spheroid with $A_R \sim 300$ will achieve $R_E = 5200$ and thus be a candidate object for the observations. One can also verify that such a needle easily satisfies the capacitative coupling limit given by Eq. (19). For $A_R = 300$, Eq. (47) is numerically evaluated (for niobium) to be

$$1.4 \times 10^{-17} \text{ s} \ \ll 8 \times 10^{-14} \text{ s}. \tag{47$'$}$$

While the slender needle concept is somewhat more plausible than the spherical shell concept, the high A_R requirement still renders it rather unlikely. (For example, an orbiting needle of 1 mm length would have a diameter of ~ 3.3 μm.)

Equilibrium Temperature

Having used f_o and Eq. (10) to establish the requisite A_R for a needle-like (niobium) object orbiting in Fig. 7, we investigate how needle size with a fixed A_R affects the equilibrium temperature. Curve a in Fig. 11, depicts the equilibrium temperature for a niobium needle as a function of a, calculated using $A_R = 300$ in Eq. (52). One sees that $a = 0.013$ cm yields $T \sim 2600$ K, somewhat below the melting point of niobium (2741 K) [6]. In this result, $b \sim 0.43$ μm. But full reality is not yet included this calculation: 1) an actual $\epsilon_r < 1$, and 2) this much heating will increase ρ_G significantly. Both of these factors will increase the equilibrium temperature. Assuming $\epsilon_r = 0.75$ and augmenting ρ_G by a factor[3] of 15, we obtain Curve b, which indicates that the equilibrium temperature drops below the melting point of niobium at $a \sim 6 \times 10^{-4}$ cm and $b \sim 2 \times 10^{-6}$ cm $= 20$ nm. That such an object would be found or could be created inside a cavity seems highly unlikely. Postulating a different material would not alter this conclusion.

Dielectric Needle

In order to determine if a dielectric needle would be possible as an orbiting object, in Fig. 12 the ratio of the Q_b of Eq. (55) to the Q_b of Eq. (41) is plotted versus ϵ, for $A_R = 300$. (As expected, the size parameter a drops out of the ratio.) From Fig. 12, one can see that the ϵ of the needle has to be very large before it has an induced electric dipole moment comparable to that of a conducting needle. Specifically, for $A_R = 300$, $\epsilon \sim 18000$ is required to obtain a polarization charge (or equivalently an induced dipole moment) of only one half of that on a similar conducting prolate spheroid. Another factor of 10 in ϵ raises this ratio to 0.9. This requirement for such a high ϵ is unrealistic and rules out a dielectric needle as a candidate for the orbiting objects.

IV. OTHER FORCES

A. Axial Force

Looking at Eqs. (3) and (6), it is evident that the Lorentz force **F** will be perpendicular to both the internal **B** and **E** fields. While, by symmetry, the **E** field along the cavity axis will be coincident with the z-axis, as soon as one considers realistic orbits going through points with $\rho > 0$, the **E** field will be characterized by radius of a curvature κ, as depicted in Fig. 13. Using geometry and Eqs. (8 and 9), one finds that the force along the z-axis,

[3]The resistivity of tungsten [14] increases by a factor ~ 18 between 20°C and 2727°C; the inequality Eq. (4) remains valid.

$$F_z = \frac{k\rho z}{\kappa}, \tag{60}$$

where $z = 0$ defines the central plane that passes through the equator of the cavity.

Eq. (60) indicates that a point characterized by $z = 0$ and $\rho \neq 0$ is a point of unstable equilibrium with respect to motion along the z-axis. When $z \neq 0$ there will be a component of force pushing the object parallel to the z-axis away from the central plane towards the nearest iris. Since this force is proportional to z, the particle will experience an exponentially accelerating axial motion. One can conclude that the longer an object is observed to remain inside the cavity, the better centered it must have been initially. The e-folding time for this motion is

$$\tau = \omega_o^{-1}\sqrt{\frac{\kappa}{\rho}}, \tag{61}$$

indicating that the most stringent z-stability test for the model will be the case which maximizes the product $t_{obs}\ \omega_o\sqrt{\bar{\rho}/\bar{\kappa}}$, where $\bar{\kappa}$ and $\bar{\rho}$ are taken to be quantities appropriately averaged over the total observation time, t_{obs}. Since $\bar{\kappa}$ and $\bar{\rho}$ enter under a square root sign, the most significant parameter is t_{obs}. In addition, the force of gravity (mentioned below) will shift and distort this plane of unstable equilibrium at $z = 0$, further reducing the probability for a long-lived (meta)stable orbit.

With respect to the z-stability of an orbiting needle, the problem is even more severe. Stability for an extended period of time is even less likely in the case of the needle because of the possibility of a rocking or precessing motion about the figure axis of the needle. Since the electrical and mechanical centers of the physical needle would not be expected to be coincident, such a motion would (almost certainly) contain some component of asymmetry that would destabilize an otherwise precisely centered needle.

Initial Alignment Requirement

In the video data associated with Ref. [1], there are two sequences of a continuing orbit with $t_{obs} > 10$ s. Looking at one of these long-lived orbit sequences, we can characterize it by $\bar{\rho} \sim 1$ cm and $f_o = 20$ Hz or $\omega_o = 40\pi$ s^{-1}. (Fig. 7 is not drawn from this sequence.) A SUPERFISH calculation of the internal $\mathbf{E}$ fields (E_z and E_ρ) in a single-cell superconducting CEBAF cavity indicates that $\bar{\kappa} \sim 50$ cm near the center of the cavity at $\bar{\rho} \sim 1$ cm. Hence, for the sake of a sample calculation, we can use $\bar{\kappa} = 100$ cm (to be conservative). Using these numbers in Eq. (61) yields

$$\tau = \frac{1}{40\pi}\sqrt{\frac{100}{1}} = 0.08 \text{ s}, \tag{62}$$

or ~ 125 e-folds in a 10 s period of observation. For the particle to remain this long within the confines of the cavity ($\mid z \mid < 5$ cm), under the influence of the z-instability force, requires that the magnitude of the initial position

$$\mid z_0 \mid \ < 5e^{-125} \sim 3 \times 10^{-54} \text{ cm}. \tag{63}$$

That at the beginning of the orbit, a particle evolving from some random process could somehow locate itself to this accuracy (with a null axial velocity) in the plane of unstable equilibrium in the center of the cavity is too improbable to be considered as plausible. And there are two examples of $t_{obs} > 10$ s.

B. Gravitational Force

One can compare a typical harmonic potential force to that of gravity. Using Eq. (9), the mass of an object satisfying the orbiting criteria in the harmonic potential is

$$M = k/\omega_o^2, \tag{64}$$

which yields a gravitational force of

$$Mg = kg/\omega_o^2, \tag{65}$$

where $g = 980$ cm/s^2 is the acceleration of gravity. Dividing this force by the (nominal) force of the harmonic potential yields

$$\frac{F_g}{F_{HP}} = \frac{kg/\omega_o^2}{k\bar{\rho}} = \frac{g}{\omega_o^2 \bar{\rho}}. \tag{66}$$

Eq. (66) indicates that F_g will be a perturbation to F_{HP}, but will not dominate it.

C. Electrostatic Force

One could imagine that an orbiting object could become electrically charged, by field emission, say. But electrostatically charged objects would be attracted toward their image charges in the walls of the cavity, leading to radial as well as axial instability. Again, this force would perturb F_{HP}, but would not dominate it.

D. Pondermotive Force

It is also known that electrically charged objects will, through nonlinear effects, experience what is called the pondermotive force, which will push the objects toward regions of smaller electric field strength. If an object, of charge q and mass M is in an electric field given by $\mathbf{E} = E_S \mathbf{1}_S \cos\omega t$, then the formula for this force is [15]

$$\mathbf{f}_{n\ell} = \frac{-q^2 \boldsymbol{\nabla} E_s^2}{4M\omega^2}. \tag{67}$$

In the 5-cell test this force offers a qualitative solution in the iris region where fields are small; however, in the single cell geometry, because the lowest fields are at the outer ends of the beam tubes, the pondermotive force will contribute to the z-axis instability of a particle centered in the cavity as well as push it radially toward the walls. Thus, it cannot be used to explain closed orbits. Moreover, explicit calculations indicate that the magnitude of $\mathbf{f}_{n\ell}$ is too small to be relevant in any case.

V. SUMMARY

A model is developed showing that in a superconducting accelerating cavity, a small particle, comprised of either a conductor or a dielectric, would have an induced oscillating electric dipole moment, and that the interaction of this oscillating moment with the local magnetic field would lead to a two dimensional potential well centered on the axis of the cavity. Thus, the model as posed leads to the possibility of closed elliptical orbits. Calculations indicate that the induced moment in dielectrics is to be too small for dielectric objects to be viable candidates, still leaving small pieces of a conducting material as candidates for the observed orbiting objects.

For conducting spheres, it was shown that the only material property contributing to the calculated orbital frequency was the material density. However, to achieve the observed orbital frequency of $\sim$80 Hz, an extremely low material density is required. A solid sphere of any known material could not satisfy this requirement. A suitable spherical shell that would be light enough to satisfy the orbital frequency requirement (much less mass, but the same induced moment) appears to be too fragile to be a reasonable possibility from a practical point of view. The conclusion is that spheres of any known material cannot, in this model, explain in the observations.

It was argued that the usual source of light associated with gas discharges, incandescent spots on a surface or electronic radiation from ionized atoms or molecules, would not be possible for the orbiting objects in such low density gasses. This left thermal heating and the consequent black (or gray) body radiation as the most likely source of luminosity. It was shown that there is plenty of power available to heat an object to incandescence. Rather, the problem is the other way around: the orbiting object had to be small enough to avoid melting.

Shedding mass by positing a needle shaped object could satisfy the orbital criteria, but the object had to be quite small to avoid melting in the conditions of the test observations. On the other hand, since the present data do not furnish information on the size or light output of the objects, a small needle cannot be completely ruled out on this basis. Niobium with its high melting point would still be a candidate material. However, to avoid melting, it was

shown that a needle of niobium would have to have a diameter of $\sim$ 40 nm. This seems much too small to be practically realized – especially by uncontrolled processes inside an accelerator cavity.

The above results are summarized in Table I; that is, there are strong arguments that it is highly unlikely that one can find a physically realizable object of any known material or shape that will satisfy the requirements imposed by the observed data as inputs to the small particle model. It also should be remarked that excluding the sphere and the needle, which effectively bracket the behavior that one would expect from other more general (and irregular) shapes, effectively excludes any general geometric shape from satisfying the orbital requirements dictated by this model.

Having noted the extreme improbability of finding an object of a suitable density and shape to yield the observed orbital frequencies, it is perhaps even more important to note that even should such object be found, the z-instability dictated by this model would render it (essentially) impossible for such an object to remain in a stable orbit for the longer periods of observation ($>$ 10 s).

VI. FUTURE AVENUES

Experimental

To proceed on the experimental front, it is important to determine the basic parameters that lead to this phenomenon. Then, as noted by Delayen and Mammosser, it would be useful to obtain spectral and intensity information on the light emitted by the orbiting objects. Stereo camera viewing, a faster camera frame rate, and better spatial resolution would be useful for orbital tracking and particle size determinations. Monitoring cavity pressure and a detailed gas analysis, as a function of time, would be also of interest.

Theoretical

The small particle model, as developed here, is clearly incomplete as a possible basis to explain the observed data. There are two specific areas that need further development:

1) The z-stability problem. The curvature of the electric field inside the cavity was shown to lead to an unstable equilibrium point in the center of the cavity, and the observed 10 s time periods of some orbits are much longer than would be possible without a mechanism to afford z-stability. It was pointed out that the force of gravity exacerbates this problem.

2) Orbital perturbations. The observed orbits were occasionally nearly perfect ellipses, but usually they manifested distortions of various kinds, *i.e.*, the class 2) "irregular-shaped closed orbits" referred to in Ref. [1]. This indicates that more than one type of force is at work, or there is a time varying force, or some nonlinear spatial force, or perhaps all of the above.

From a theoretical perspective, it would be of gratifying if these questions could be understood. A model of wider scope needs to be developed. However, to find the path to this wider scope poses a significant challenge.

Finally, while it was not covered in this paper, it is worth noting that the transient and diffuse luminosity or "flash of light" [1], which often precedes the onset of orbiting cavity lights, is also worth study. It might be due to a burst of ionized gas released into the cavity, or, more intriguing, it may be a new physics phenomenon in its own right. Intensity, spectral content, and time waveforms associated with this light would assist in an evaluating this question.

ACKNOWLEGEMENTS

I would like to thank J. R. Delayen and J. Mammosser for generously sharing the video data taken in conjunction with Ref. [1], and for numerous useful conversations. In addition, I wish to thank J. Mammosser for furnishing the relevant SUPERFISH calculations of the internal cavity fields. I would also like to thank P. Wilson for a useful conversation and a relevant reference and I. Wieder for useful conversations.

References

[1] J. R. Delayen and J. Mammosser, *Proceedings of the 1999 Particle Accelerator Conference*, New York, p. 925.

[2] J. D. Jackson, *Classical Electrodynamics* (J. Wiley & Sons, Inc., New York and London, 1962), p. 611.

[3] *Ibid.,* p. 34.

[4] *Ibid.,* p. 115.

[5] *Ibid.,* p. 620.

[6] J. Emsley, *The Elements, 2^{nd} Ed.* (Clarendon Press, Oxford, 1991).

[7] W. R. Smythe, *Static and Dynamic Electricity* (McGraw Hill Book Co., Inc., New York, Toronto, and London, 1950), p. 165, *et seq.*

[8] *Ibid.,* Eq. 5.281 (1).

[9] J. D. Jackson, *op. cit.,* p. 9.

[10] R. B. Leighton, *Principles of Modern Physics* (McGraw Hill Book Co., Inc., New York, Toronto, and London, 1959), p. 62.

[11] W. R. Smythe, *op. cit.,* p. 208.

[12] M. Cantin, M. Casse, L. Koch, R. Jouan, P. Mestreau, D. Roussel, F. Bonnin, J. Moutel, and S. J. Teichner, *Nuc. Inst. Meth.,* **118**, 177 (1974).

[13] Particle Data Group, *The Eur. Phys. Jour. C,* **3**, 76 (1998).

[14] C. D. Hodgeman, Ed. in Chief, *et al., Handbook of Chemistry and Physics,* 41^{st} Ed. (Chemical Rubber Publishing Co., Cleveland, OH, 1959) p. 2595.

[15] F. F. Chen, *Introduction to Plasma Physics* (Plenum Press, New York and London, 1974), p. 257.

Table I

CANDIDATE	COMMENTS
Conducting Sphere:	Too heavy to achieve observed orbital frequency.
Conducting Spherical Shell:	Too fragile to be practically realized.
Dielectric Sphere:	Too heavy to achieve observed orbital frequency.
Dielectric Spherical Shell:	Induced electric dipole moment too small to achieve observed orbital frequency.
Conducting Needle:	Must have a high aspect ratio to achieve observed orbital frequency. Must be of small size and of a material of high enough melting point to yield observed luminosity through black (or gray) body radiation without melting. The probability of such an object in the cavity seems highly unlikely.
Dielectric Needle:	Must have a high aspect ratio to achieve observed orbital frequency, which in turn requires an unrealistically high dielectric constant.

FIGURE CAPTIONS

1. A sphere of radius a in a uniform field E_z. The induced electric dipole $\boldsymbol{\mu}$ is indicated.

2. Modeling a resistive sphere with a geometry suitable for a lumped component equivalent circuit. The resistivity of the sphere is lumped into a discrete resistor connecting the two conducting hemispheres.

3. Equivalent circuit of the resistive sphere model (Fig. 2) used for a power and luminosity analysis.

4. A sphere of radius a with an incremental slice of thickness Δz indicated. The angle θ gives the location of the slice.

5. Prolate spheroidal boss, of semi-axes a and b, protruding from a ground plane. Using the symmetry in the ground plane, this geometry properly represents a floating or orbiting prolate spheroid embedded in, and aligned with, a uniform electric field E_z along the z-axis.

6. A prolate spheroid with an incremental slice of thickness Δz indicated. This Δz slice intersects the surface of the spheroid ($\eta = \eta_0$) at ξ.

7. A reproduction of Fig. 2a of Ref. [1], depicting a closed elliptical orbit segment. The major axis of the ellipse is indicated. Points A and B denote the termini of the orbital segment as determined by variations in the track luminosity.

8. The sine wave variation of the orbit along the major axis of the elliptical orbit. The locations of points A and B that are derived from Fig. 7 are indicated.

9. A plot versus A_R of the induced moment of a prolate spheroid normalized to that of a sphere for the same a. The induced moment drops as A_R increases, but not as fast as the volume drops.

10. A plot versus A_R of the geometric enhancement factor R_E of the prolate spheroid relative to a sphere. R_E includes both the reduction in the induced moment and the reduction in volume as A_R increases. It can be seen that an R_E of ~ 5200 dictates a prolate spheroid characterized by $A_R \sim 300$.

11. Plots of the equilibrium temperature versus the major semi-axis a of a niobium needle with $A_R = 300$. Curve a was calculated using the resistivity $\rho_\Omega = 12.5$ $\mu\Omega$-cm, the resistivity of niobium at 273 K, as input. The point at $a = 0.013$ cm and T = 2600 K is indicated. Because resistivity increases significantly with temperature, Curve a is well below what would actually be expected. Curve b was calculated using the resistivity of $\rho_\Omega = 187.5$ $\mu\Omega$-cm, the estimated resistivity of niobium at $\sim$2600 K. Also, $\epsilon_r = 0.75$, an estimated emissivity, was used. The point at $a \sim 6 \times 10^{-4}$ cm and T = 2600 K is indicated. A dashed line is depicted to indicate an estimate of the effect of the

change in resistance with temperature, assuming that the point at 2600 K is a proper estimate. As one goes to smaller a, the equilibrium T will drop, tending to bring the actual curve closer to Curve a.

12. Assuming $A_R = 300$, a plot as a function of dielectric constant ϵ of the ratio of the polarization charge induced on a dielectric prolate spheroid with respect to that on a conducting prolate spheroid. As one would expect for a large A_R, ϵ must be exceptionally large for the moment of a dielectric spheroid to approach that of a conducting spheroid.

13. A depiction of the curvature of the $\mathbf{E}$ field inside the accelerating cavity, which is shown in the text to lead to an unstable equilibrium with respect to z-axis motion. The radius of curvature, κ, is indicated.

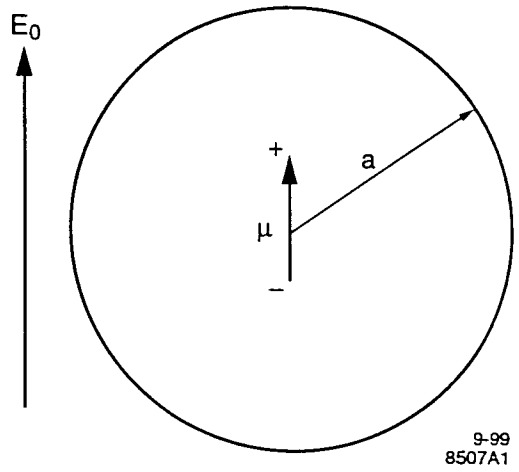

Fig. 1

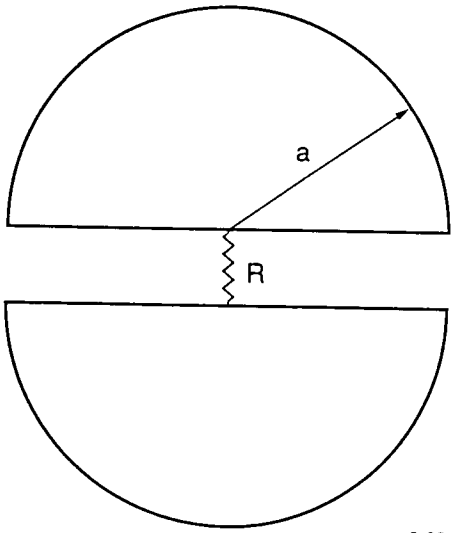

Fig. 2

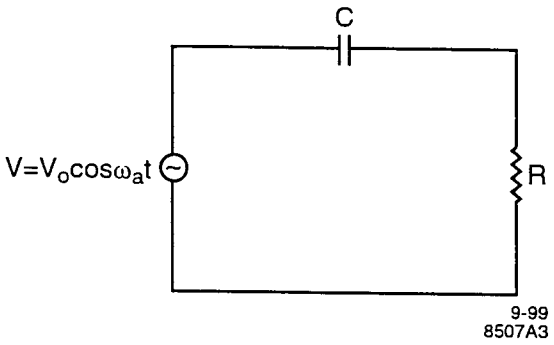

Fig. 3

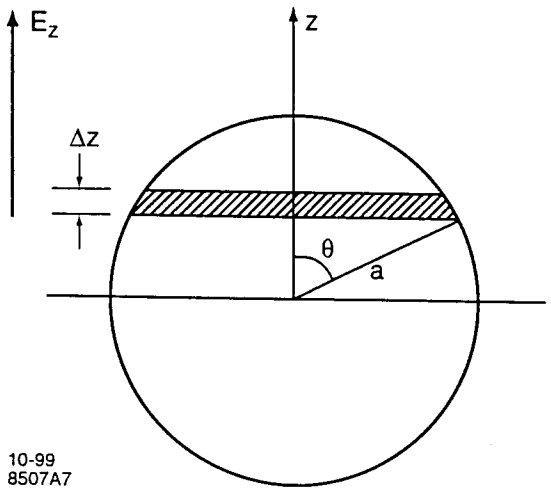

Fig. 4

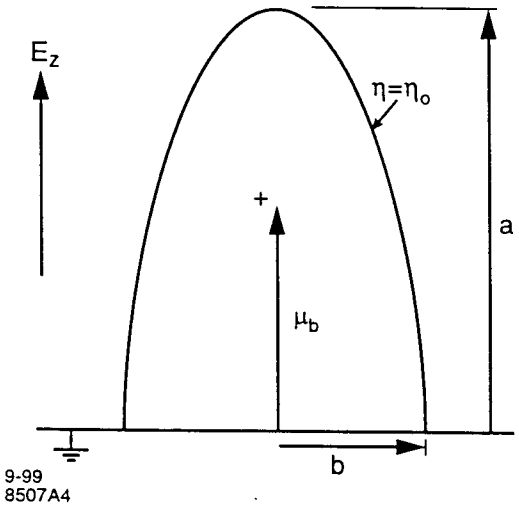

Fig. 5

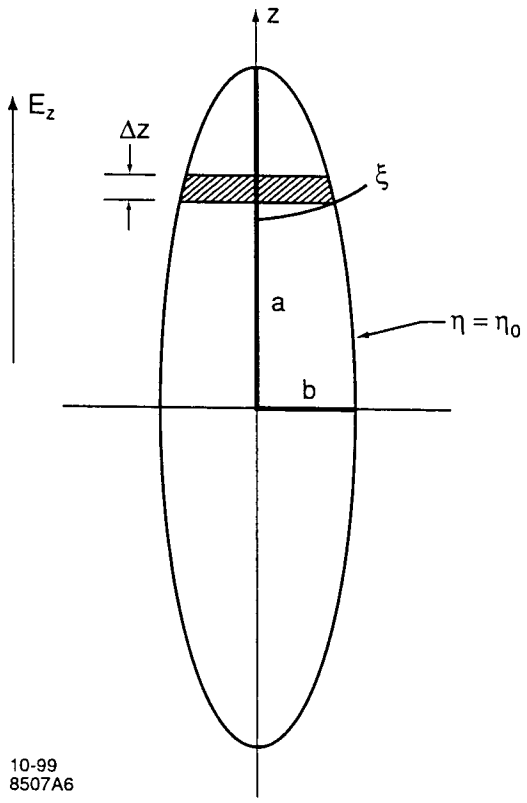

Fig. 6

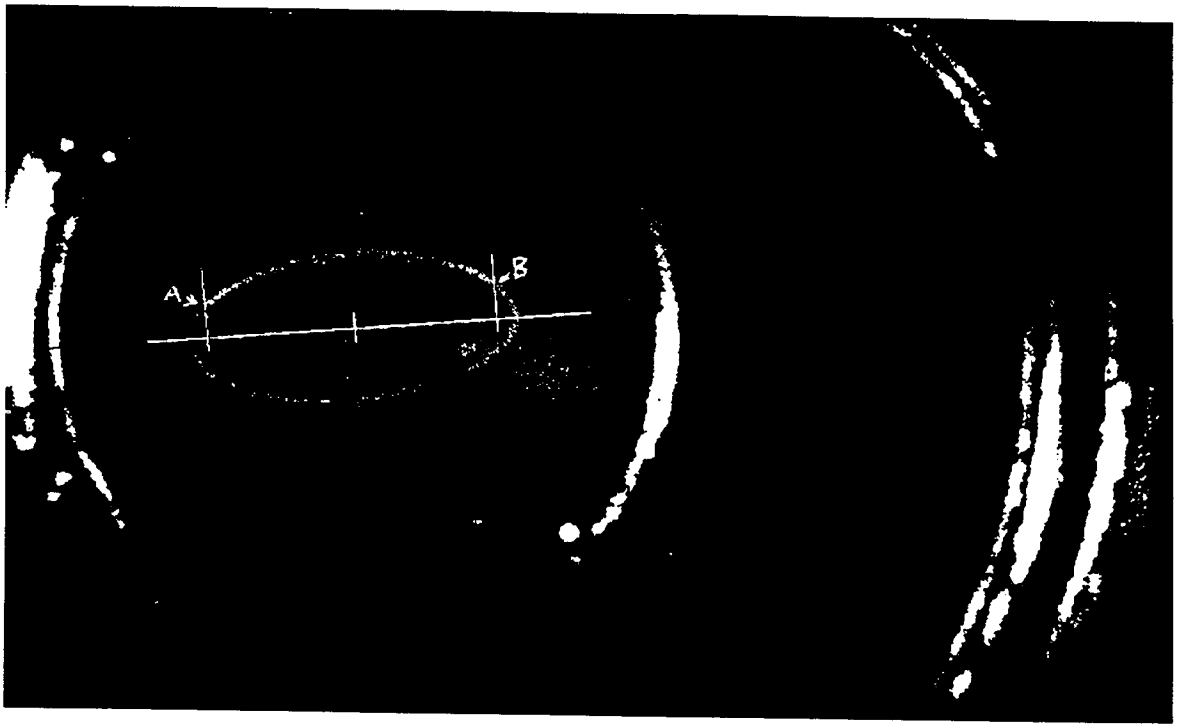

12-99
8507A15

Fig. 7

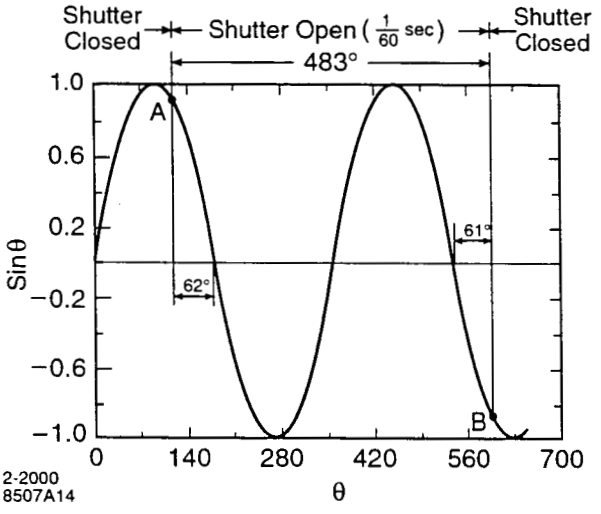
Shutter Closed
Shutter Open (1/60 sec)
Shutter Closed
483°
1.0
0.6
0.2
−0.2
−0.6
−1.0
Sinθ
A
B
62°
61°
0
140
280
420
560
700
θ
2-2000
8507A14

Fig. 8

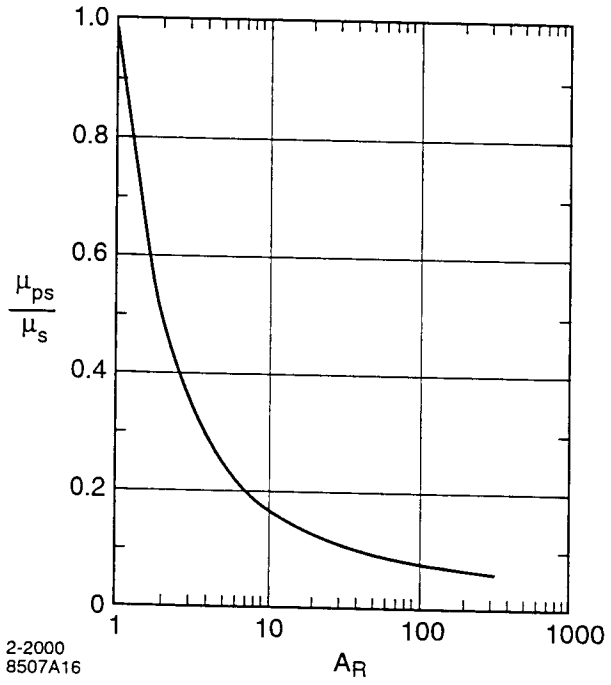

Fig. 9

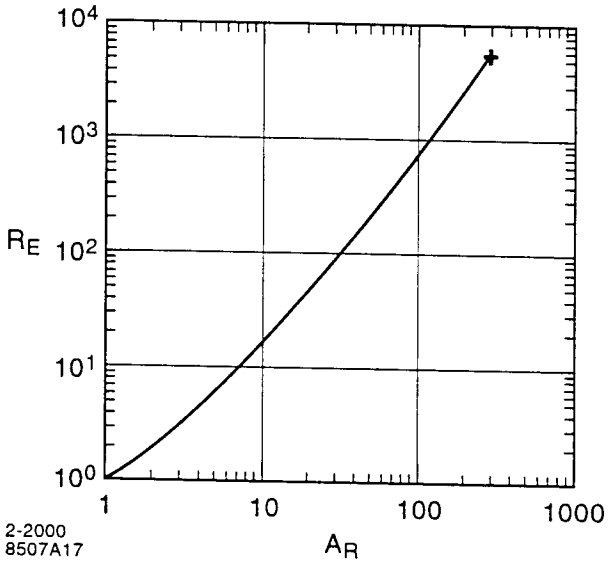

Fig. 10

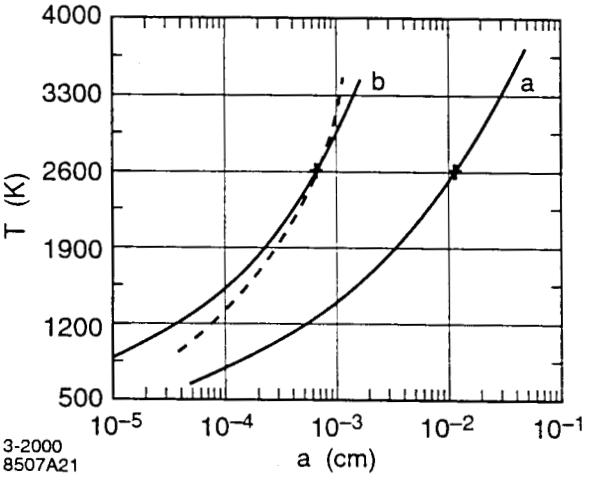
4000
3300
2600
1900
1200
500
T (K)
b
a
10^{-5}
10^{-4}
10^{-3}
10^{-2}
10^{-1}
a (cm)
3-2000
8507A21

Fig. 11

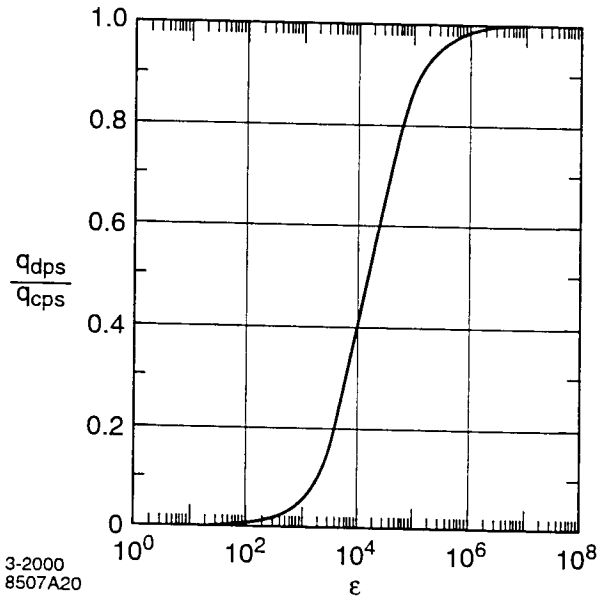
1.0
0.8
0.6
$\frac{q_{dps}}{q_{cps}}$
0.4
0.2
0
10^0
10^2
10^4
10^6
10^8
ε
3-2000
8507A20

Fig. 12

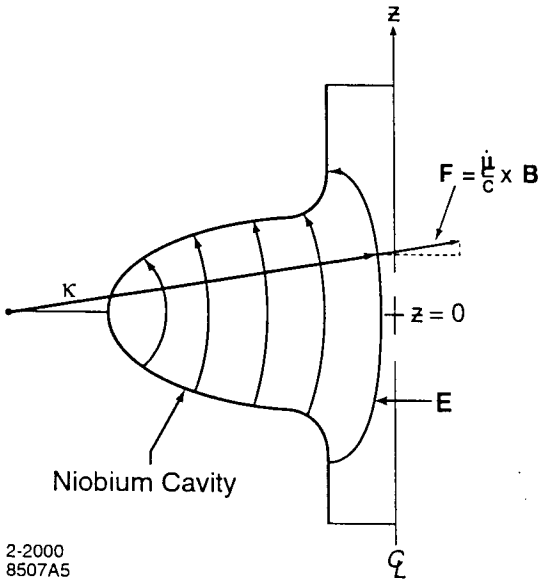

Fig 13